

Simulation and Experimental Research into Combined Electrochemical Milling and Electrochemical Grinding Machining of Ti40 Titanium Alloy

Xizhong Wang, Hansong Li* and Shen Niu

College of Mechanical and Electrical Engineering, Nanjing University of Aeronautics and Astronautics, Nanjing, 210016, China

*E-mail: hsli@nuaa.edu.cn

Received: 18 October 2019 / *Accepted:* 21 August 2020 / *Published:* 30 September 2020

Ti40 titanium alloy is a typical difficult-to-cut material with high tensile strength and toughness. To achieve both high efficiency and high precision, this paper proposes a machining method combining electrochemical milling for rough machining and electrochemical grinding (ECG) for finish machining. Instead of the conventional tool used in electrochemical milling, which has a sharp edge, the tool used had a rounded corner, which increases machining efficiency. The simulation shows that the current density for this tool is weaker at the corner of the machined slot. Slots were cut via rough machining by electrochemical milling. The polarization and current efficiency for Ti40 titanium alloy in 10 wt.% NaNO₃ electrolyte were measured. The experimental results show that the maximum feeding rate for electrochemical milling of Ti40 increased from 1.5 to 1.7 mm/min. The cuts were 3 mm deep and the material removal rate was 21.2 mm³ min⁻¹. The sidewalls of the machined slots were finished with ECG. Only a small amount of material was removed and there was no overcut. The average sidewall flatness and surface roughness decreased from 109.7 to 59.0 μm and from 5.089 to 0.789 μm. The oxidation film formed during the rough machining had been removed.

Keywords: Ti40 titanium alloy; Electrochemical milling; Electrochemical grinding; Flatness; Surface roughness

1. INTRODUCTION

Ti40 is a titanium alloy widely used in aero-engine manufacturing because of its flame-retardant properties and high-temperature performance. However, due to its high strength and low thermal conductivity, Ti40 is a difficult-to-machine material. Conventional machining of Ti40 suffers from severe tool wear, poor surface quality, and low productivity[1-3]. Furthermore, the complexity of aero-engine components and the large amount of material that needs to be removed for them make

manufacturing more difficult[4-6]. Owing to these limitations, conventional machining is not adequate for the modern aerospace industry. Hence, finding a method of machining Ti40 titanium alloy with low cost, high efficiency, and high flexibility is necessary and essential.

Electrochemical machining (ECM) removes material efficiently by anodic dissolution. There is no tool wear, no residual stress, no machining deformation, and no effects due to heating. However, traditional ECM is a form of copy machining and it requires expensive tools that are time-consuming to design for complex components[7-9]. In contrast, electrochemical milling uses a cathode with a simple shape—generally a rod or sphere—to form a surface along its path of movement, which is controlled by a numerical control (NC) system. By integrating the capabilities of ECM and the flexibility of NC technology, electrochemical milling can be utilized to machine complex components. In recent years, to remove large amounts of difficult-to-cut material, inner-jet electrolyte supply mode and plunge electrochemical machining have been developed. Liu et al. [10]. used an irrotational spherical cathode with an electrolyte outlet to manufacture a lead ball nut raceway in a GCr15 steel workpiece with a machining depth of 2.5 mm and a feed rate of 0.3 mm/min. Niu et al. [11]. employed a rotating dead-end tube electrode with six electrolyte outlets on the tool sidewall during electrochemical milling of Inconel 718, in which a cut of depth 3 mm and a feed rate of 2.1 mm/min were achieved. They further found that, compared with a spherical cathode, a tubular cathode with some tool-sidewall outlets was able to achieve higher feed and material removal rates.

In general, electrochemical milling is effective for difficult-to-cut materials. However, undesirable dissolution, which is known as stray removal [12,13], is unavoidable. Consequently, the machining accuracy of electrochemical milling is poor and the profile of the machined surface is usually uneven. Therefore, subsequent surface finishing is necessary.

Electrochemical grinding (ECG) produces surfaces that are less rough. ECG is a hybrid machining process that combines ECM and mechanical grinding by coating the surface of the rotary cathode with abrasive grains. In ECG, the cathode tool rotates at high speed to remove material electrochemically and mechanically. Compared with mechanical grinding, ECG requires a smaller grinding force and there is less low tool wear because the oxidation film, which is generated by the electrochemical reactions and covers the machining surface, is softer than the workpiece and is easier to remove [14,15]. Hasçalık and Çaydaş [16] used ECG for shallow cuts of depth 50 μm with a high feed rate of 6 mm/min to improve the surface roughness and to eliminate defects on the surface of titanium alloy Ti-6Al-4V that had already been machined by electrical discharge machining. Using ECG for titanium alloy Ti-6Al-4V, Li et al. [17] successfully produced a surface with roughness $Ra = 0.4 \mu\text{m}$ using a grinding wheel with a diameter of 1.8 mm. Zhu et al. [18] used a rod with an abrasive coating as a grinding wheel to process the surfaces of small pre-machined holes of stainless steel 321 with diameters of 0.6 mm. The machined surfaces were smoother, with $Ra = 0.5 \mu\text{m}$. Clearly, ECG can be used for surface finishing after electrochemical milling.

In summary, electrochemical milling achieves efficient removal of difficult-to-cut materials, after which ECG can be used for finishing machining. Obviously, a method that combines electrochemical milling and ECG has the potential to achieve both high efficiency and high precision for difficult-to-cut materials. In electrochemical milling—the first stage of this combined method—a high feed rate can improve processing efficiency and shorten the manufacturing cycle. However, in the

studies mentioned above, the cathode sidewall and bottom were connected by a sharp corner. It is worth noting that we have found that the presence of a sharp corner imposes a limit on how much the feed rate of a tubular cathode can be increased, owing to sparking at the corner [11]. Besides, this combined method has not previously been reported for Ti40 titanium alloy.

In this paper, we propose an innovative machining process for Ti40 titanium alloy that combines electrochemical milling followed by ECG to remove material efficiently with good surface quality. First, we describe the combined method. To increase the maximum feed rate in electrochemical milling, we propose a tubular tool with a rounded corner connecting the sidewall and bottom of the tool. We then conduct an electric field simulation and discuss its results with the aim of explaining the advantage of a rounded corner. In addition, we investigate the ECM characteristics of Ti40 titanium alloy. Subsequently, we examine the maximum feed and material removal rate of electrochemical milling at different applied voltages. Finally, we compare the cross-sectional profiles, flatness, roughness and surface morphologies produced by the two stages.

2. MATERIALS AND METHODS

2.1 Combined Electrochemical Milling and ECG

The combined machining process has two stages: (1) electrochemical milling as rough machining and (2) ECG as finish machining (Fig. 1.).

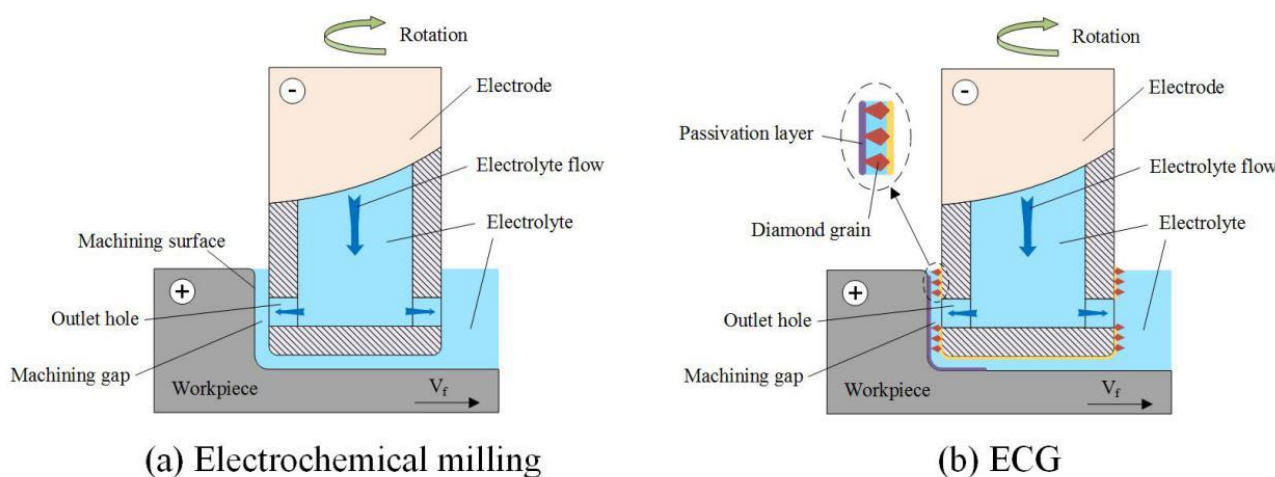


Figure 1. Schematic of (a) electrochemical milling and (b) ECG

During electrochemical milling, the electrode removes metallic material while moving along a path controlled by an NC system and rotating rapidly. Electrolyte flowing from inside the electrode into the machining gap through the outlet holes establishes a persistent electrochemical circle. Electrochemical reaction products along with heat are carried off by the flow of electrolyte. To break down the oxidation layer generated on the machining surface, a relatively high applied voltage, above

the dissolution potential of the material, is usually used. However, stray removal enhanced by the high applied voltage makes the profile uneven. To improve the machining accuracy and surface quality, ECG is subsequently applied as surface finishing. ECG is a form of electrochemical milling in which the tool electrode is coated with abrasive grit, generally diamond. The main function of the abrasive grit is to remove the inactive but soft oxidation layer produced by the electrochemical dissolution and thus to expose fresh metal for further electrochemical reactions. Hence, in ECG, the applied voltage is lower than the dissolving potential of the material to maintain the generation of the oxidation layer.

2.2. Electrical Field Simulations

In electrochemical milling, the maximum feed rate is an important index as it reflects the machining efficiency. However, the maximum feed rate is impacted by the distribution of the electric field. A simulation was used to analyze the electric field in the inter-electrode gap.

2.2.1 Physical Model

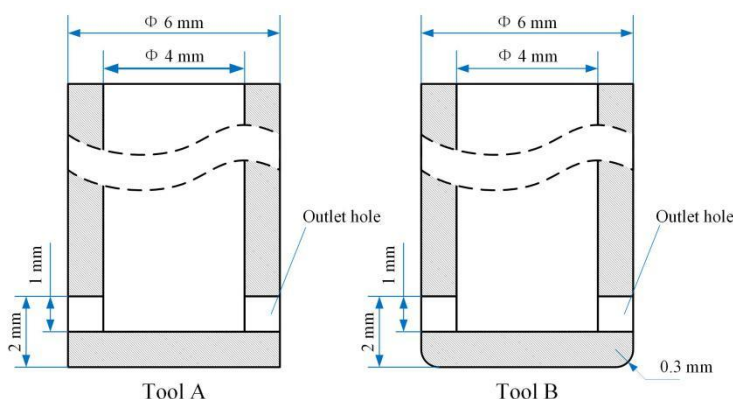


Figure 2. Dimensions of two electrochemical milling tools, one with sharp corners and one with rounded corners

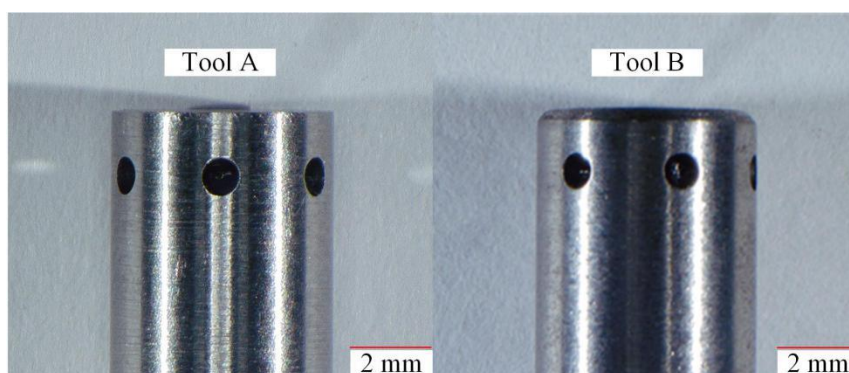


Figure 3. The two different electrochemical milling tools, A and B

The aim of the electrical field simulation was to calculate the distribution of the current density in the machining gap. The dimensions of two inner-jet electrochemical milling tools—tool A with sharp corners and tool B with rounded corners—are shown in Fig. 2. And Fig. 3. The outside and inside diameters of both tool A and tool B were 6 mm and 4 mm, respectively. Tool B has a corner of radius of 0.3 mm between the sidewall and the bottom of the tool. Both tools had six small holes with a diameter of 1 mm arranged symmetrically on the sidewall.

Since they hardly affect the electrical field, the outlet holes were ignored in the simplified physical models, which are shown in Fig. 4. Cross section A of the tools is used to illustrate the details of the models. The following assumptions were made:

- (1) The current density distribution on the cathode is dominated by Ohmic effects.
- (2) The conductivity of the electrolyte, κ , is constant.
- (3) The concentration gradient in the bulk electrolyte is negligible.
- (4) The conductive areas of the anode and cathode surfaces are equipotential surfaces.

Based on ECM shaping theory, the electric potential, ϕ , in the interelectrode gap Ω is governed by Laplace's equation [19,20] :

$$\Omega: \nabla^2\phi = \frac{\partial^2\phi}{\partial x^2} + \frac{\partial^2\phi}{\partial y^2} = 0 \quad (1)$$

The boundary conditions are

$$\phi|_{\Gamma_{1,2}} = U \quad (\text{at the anode surface}) \quad (2)$$

$$\phi|_{\Gamma_{4,5,6,7}} = 0 \quad (\text{at the cathode surface}) \quad (3)$$

$$\frac{\partial\phi}{\partial n}|_{\Gamma_{3,8,9}} = 0 \quad (\text{the boundary condition}) \quad (4)$$

where U is the applied voltage and n is the unit vector normal to the surface.

The current density, i , is

$$i = \kappa\nabla\phi \quad (5)$$

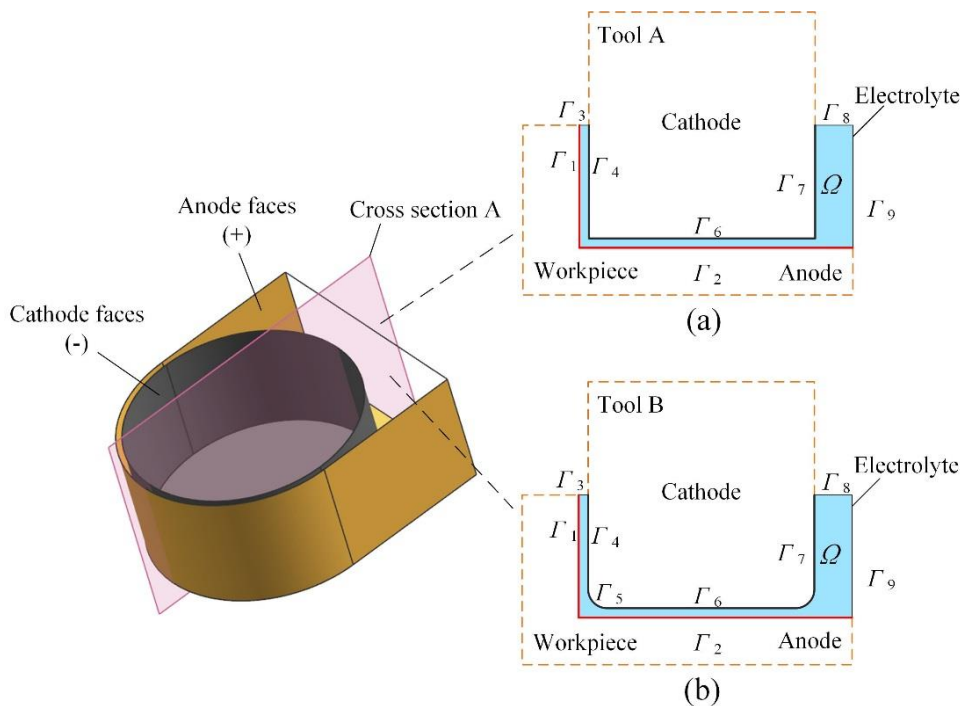


Figure 4. Simplified physical models of (a) tool A and (b) tool B

2.2.2 Simulation Conditions and Analysis of Simulation Results

Using COMSOL Multiphysics, a finite-element method was employed to calculate the current density. The simulation parameters are listed in Table 1.

Table 1. Simulation parameters

Parameter	Value
Applied voltage (V)	15
Electrolytic conductivity (S/m)	10
Inter-electrode gap (mm)	0.2

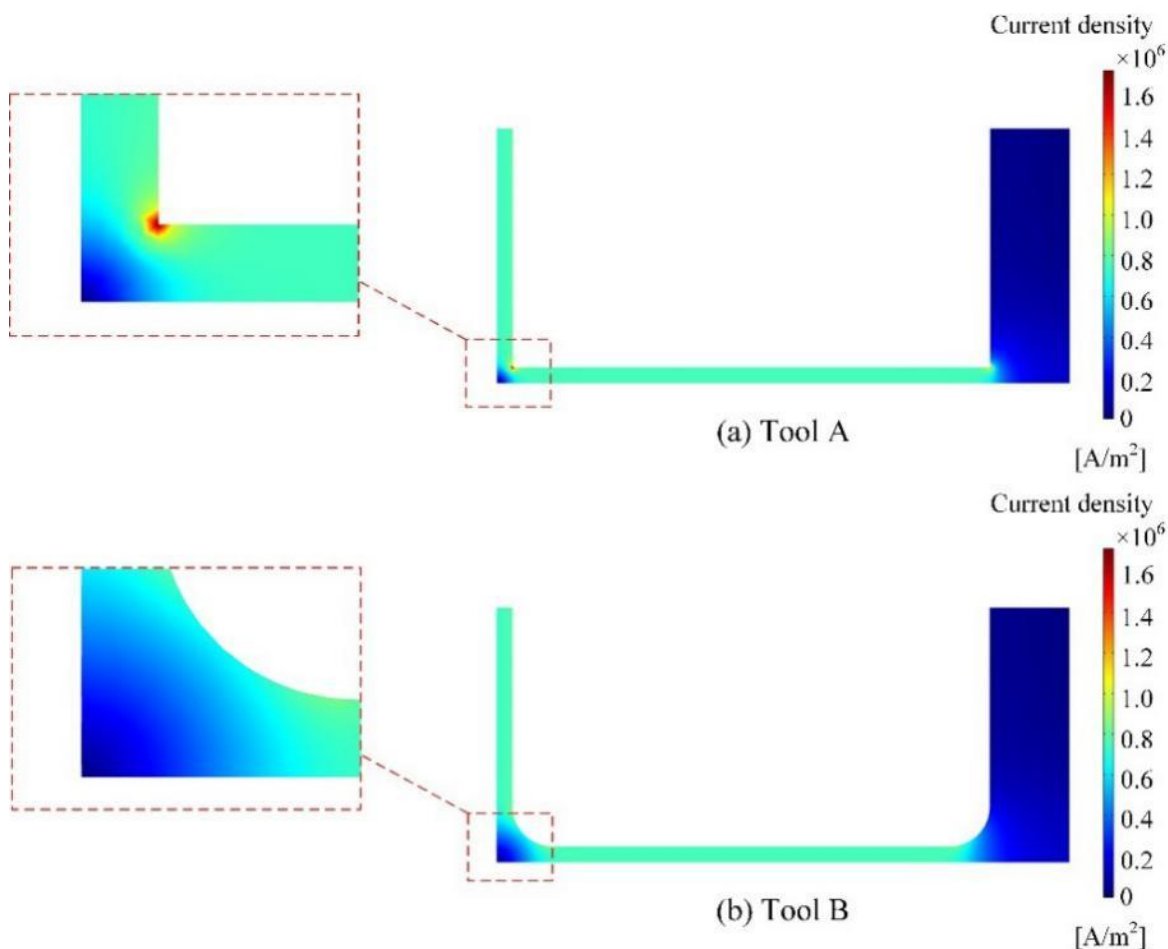


Figure 5. Electric field distribution at the bottom of the tools

Fig. 5. shows the results of the current density simulation for the cross sections A. For tool A (Fig. 5a), there is a region near the corner of the anode surface between the sidewall and the bottom of the anode in which the current density is relatively low. In general, the material dissolution rate is

positively correlated to the current density. Therefore, the amount of material removed in this region is less than elsewhere, inevitably resulting in a workpiece with a rounded corner. Fig. 6. demonstrates the effect of this rounded corner on the maximum feed rate. As the tool is fed, the part of the tool closest to the corner of the workpiece is the sharp edge, because the inter-electrode gap here is the smallest. When the feed rate is too high, the equilibrium between tool feed rate and material dissolution breaks and the anode and cathode come into physical contact. A spark occurs, which damages both the tool and the workpiece. The discussion above explains why the spark is most likely to occur at the corner of the tool.

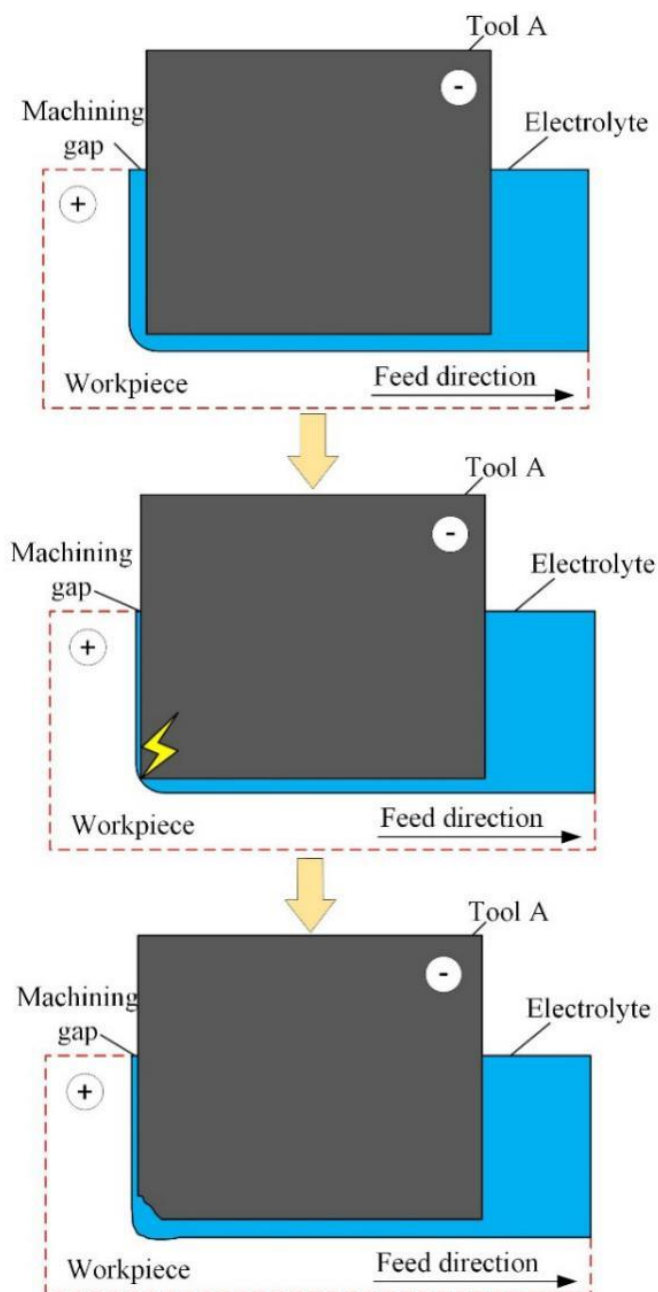


Figure 6. Sparking

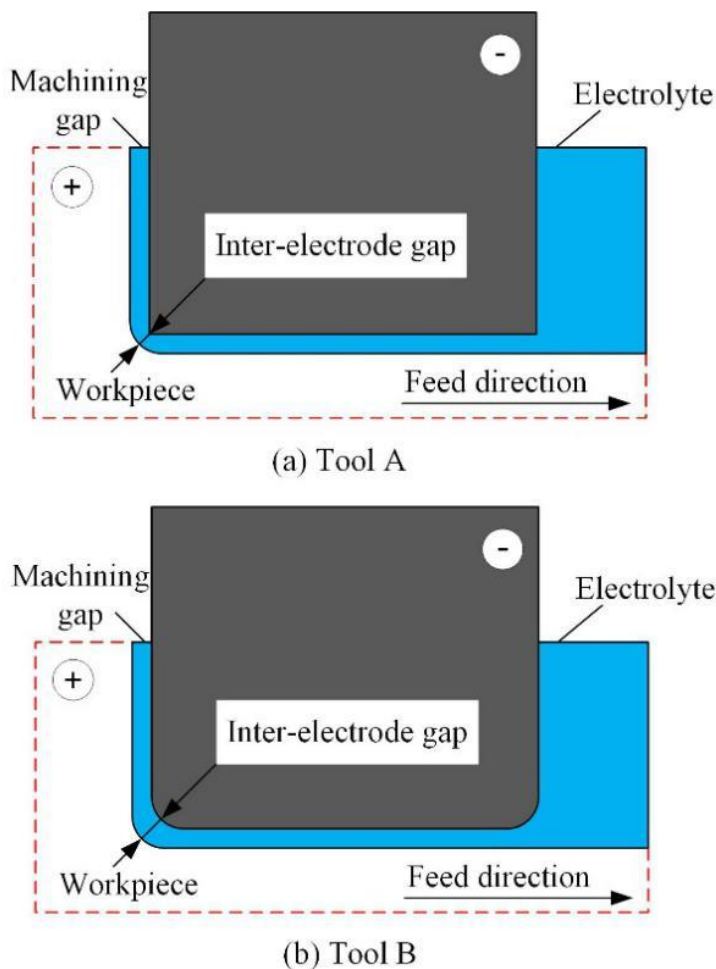


Figure 7. Inter-electrode gap

For tool B (Fig. 5b), there is a similar region with a low current density. The simulation indicates that the shape and size of the corner in the slot machined with tool B are almost identical to those for a corner machined with tool A.

According to the theory of ECM, the inter-electrode gap Δ can be expressed as [21,22]

$$\Delta = \frac{\eta \omega \kappa (U - \delta E)}{v_f} \quad (6)$$

where η is the current efficiency, ω is the volume electrochemical equivalent, κ is the electrolytic conductivity, U is the applied voltage, δE is the polarization potential and v_f is the feed rate. From equation (6), it can be seen that with an increasing cathode feed rate, the size of the inter-electrode gap decreases. For tool A, when the feed rate reaches its maximum, the inter-electrode gap can no longer be reduced, otherwise sparking will occur. However, since tool B has rounded corners, unlike tool A, which has a sharp edge, the inter-electrode gap at the corner is larger, as shown in Fig. 7. When the feed rate of tool B reaches the maximum feed rate of tool A, the inter-electrode gap can be further reduced by increasing the feed rate. Thus, in theory, the maximum feed rate of tool B is higher than that of tool A.

2.3. Experimental Procedures

2.3.1 Preparation of Samples and Electrolytes

The chemical composition of Ti40 alloy is listed in Table 2. Experiment samples were cut into small cubes ($10 \times 10 \times 10$ mm) by wire electrical discharge machining, and the surfaces of the cubes were polished with metallographic sandpaper. After being degreased with acetone and rinsed with deionized water, all samples were dried with clean compressed air. All experiments were conducted in NaNO_3 solution. Analytical reagent grade NaNO_3 was used to obtain the 10 wt.% NaNO_3 electrolyte.

Table 2. Chemical composition of Ti40 alloy

Elements	V	Cr	Si	C	Fe	O	N	H	Ti
Composition	25.4	16.8	0.26	0.0	0.1	0.1	0.02	0.0	Balanc
(wt.%)				8	7	1		1	e

2.3.2 Potentiodynamic Polarization Measurements

Polarization measurements were performed with an electrochemical workstation (Zennium E, Zahner, Germany). A platinum net was used as the counter electrode, and all potentials were measured against a saturated calomel electrode. Prior to making the measurements, the oxidation film was removed from the working electrode at -1 V for 60 s and the surface was stabilized at E_{ocp} for 30 min. The potential scan rate was 10 mV/s. Polarization measurements were carried out in 10 wt.% NaNO_3 solution at $30 \pm 1^\circ\text{C}$ three times.

2.3.3 Current Efficiency Measurements

The current efficiency is defined as

$$\eta = M/KIt \quad (7)$$

where M is the mass dissolved from the sample (g), K is the theoretical mass electrochemical equivalent ($\text{gA}^{-1}\text{s}^{-1}$), I is the current between the anode and cathode (A), and t is the machining time (s).

When making the measurements, the electrochemical reaction occurred under constant current density. The machining time was recorded, the weight loss of the sample was measured, and then the current efficiency was calculated using equation (7). All the experiments were conducted in 10 wt.% NaNO_3 solution at $30 \pm 1^\circ\text{C}$.

2.3.4 Combined Electrochemical Milling and ECG

Fig. 8. illustrates the main components of the ECM system: machining body, NC system (computer and motion control card), power supply, electrolyte circulation system, and data acquisition system. The machining tool moves through four axes: three linear axes X , Y , and Z , and a rotary axis C .

During processing, tool movement was precisely controlled by a motion control card through a computer, and the pressure of electrolyte was stabilized by a pressure control valve. The cleanliness and temperature of the electrolyte were maintained with a filter and heat exchanger, respectively.

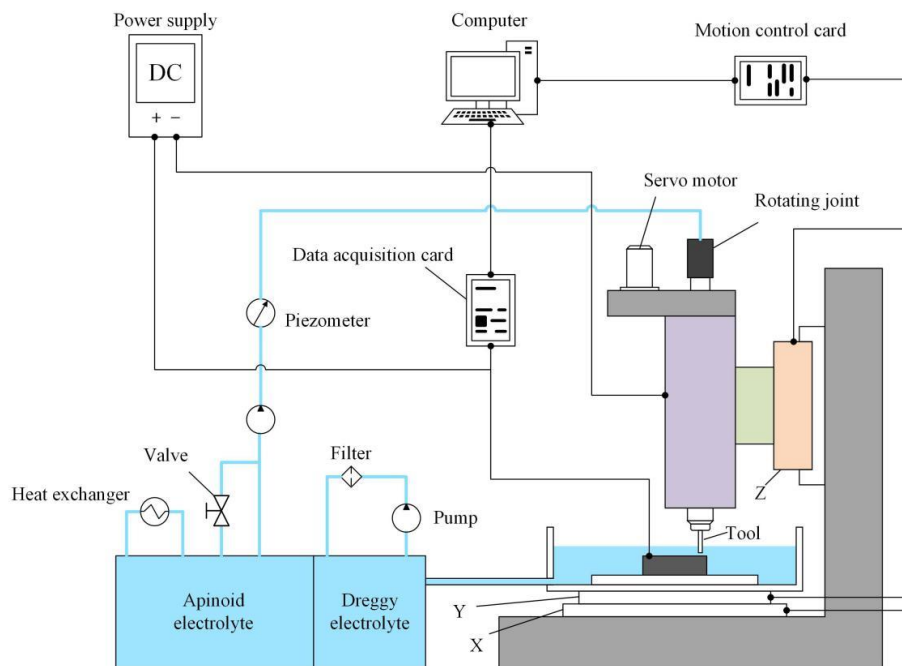


Figure 8. Schematic diagram of the ECM system

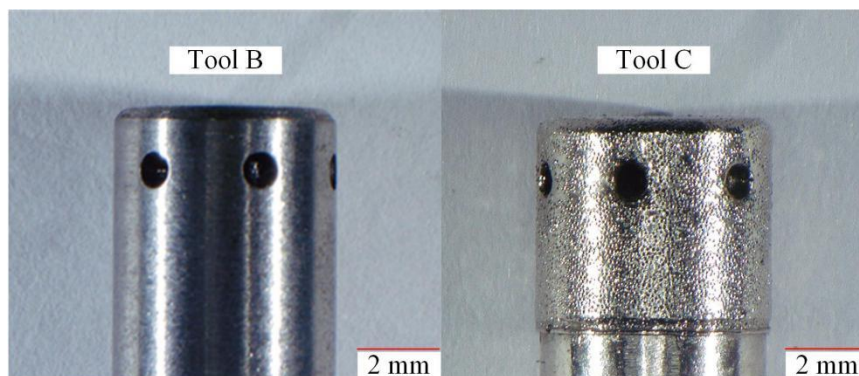


Figure 9. Electrochemical milling tool B and ECG tool C

Tool B was used for electrochemical milling and tool C for ECG (Fig. 9.). Tool C was produced from tool B by coating the sidewall and bottom surface of the tool with an abrasive diamond grit through electroplating. The particle size and concentration of the diamond were approximately 75–90 μm and 8.8 carat cm^{-3} , respectively. The average diameter of tool C was 6.2 mm.

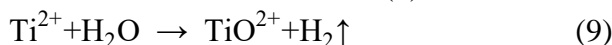
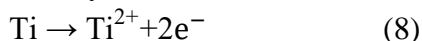
2.3.5 Measuring Machining Quality

The machining quality of electrochemical milling and ECG was checked. Cross-sectional photographs of the machined slots were captured with an optical microscope (DVM5000, Leica, Germany). The cross-sectional profiles were measured with a coordinate measuring instrument (Zeiss Contura, Germany). The corrosion morphology was studied with a scanning electron microscope (SEM; S-4800N, Hitachi, Japan). A 3D scanning laser microscope (OLS4100, Olympus, Japan) was used to measure the surface roughness of the slot sidewalls. All samples were cleaned with deionized water and then acetone before being measured.

3. RESULTS AND DISCUSSION

3.1 ECM Characteristics

The polarization curve for Ti40 (Fig. 10.) shows that the current density gradually increases once the applied potential exceeds approximately 4.5 V. This is the dissolution potential. The polarization curve suggests that a passivation layer, which is corrosion-resistant but soft, forms on the surface of the material if the voltage applied is less than 4.5 V. The main element that affects the formation of the passivation layer of Ti40 is Ti. The anodic passive reactions can be summarized as follows [23,24]:



A small number of bubbles are adsorbed on the surface of the platinum net, which indicates that the cathode has undergone a chemical reaction:



Rapid corrosion and dissolution of the material occur once the voltage applied is greater than about 4.5 V. The rapid dissolution of the metal body of the anode sample may be summarized as follows [25]:



For larger voltages, the current density grows rapidly as the potential increases, indicating that the rate of metal dissolution is positively correlated with the applied voltage.

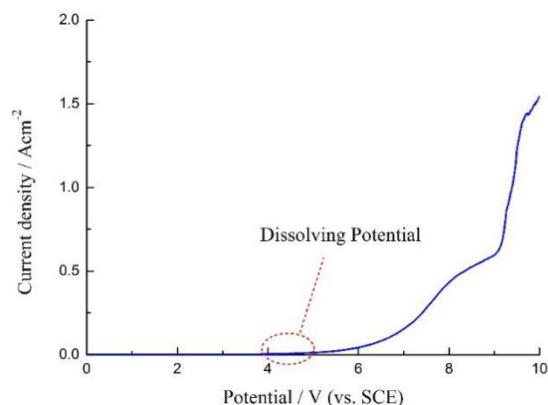


Figure 10. Polarization curve of Ti40 in 10 wt.% NaNO₃ electrolyte at 30°C

The current efficiency curve of Ti40 is plotted in Fig. 11. The current efficiency increases rapidly when the current density is less than 1 A cm⁻², and then becomes stable at around 92% once the current density exceeds about 5 A cm⁻².

Thus, for Ti40, a voltage greater than the dissolution potential should be used for rough machining because of the high speed and high current efficiency. In contrast, to maintain the formation of the passivation film, a voltage under the dissolution potential should be used for finishing machining [26]. Furthermore, the relatively low voltage reduces stray current attacks and tool wear, and consequently the surface quality is better. In our research, the voltages applied for electrochemical milling and for ECG were 15 V and 1 V, respectively.

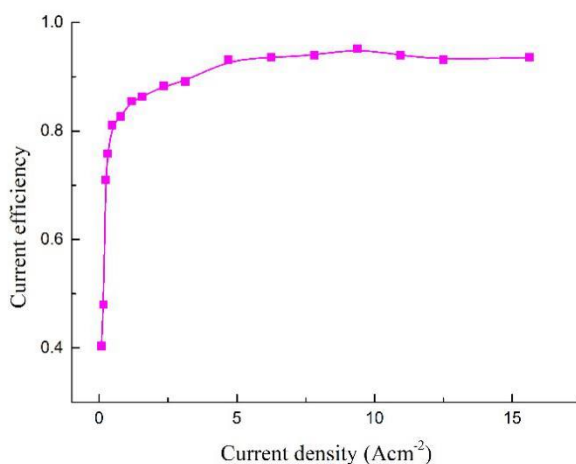


Figure 11. Current efficiency curve of Ti40 in 10 wt.% NaNO₃ electrolyte at 30°C

3.2 Comparison of Machining Performance

In this section, the machining performance of electrochemical milling and ECG is demonstrated and discussed. The machining parameters are listed in Table 3.

Table 3. Parameters used in electrochemical milling and subsequent ECG

Parameter	Electrochemical milling	ECG
Applied voltage (V)	15	1
Electrolyte pressure (MPa)	0.6	0.3
Electrolyte concentration (wt.%)	10%	10%
Electrolyte temperature (°C)	30	30
Spindle speed (rpm)	1000	1000
Feed rate (mm min ⁻¹)	1.7	15
Depth of cut (mm)	3	0.015

First, the maximum feed rates for electrochemical milling using tools A and B at a depth of cut of 3 mm using an applied voltage of 15 V and electrolyte pressure of 0.6 MPa were determined. Slots were machined under a relatively high voltage and electrolyte pressure to obtain a high material removal rate (MRR), which is a measure of machining efficiency:

$$MRR = \frac{\Delta V}{t} \quad (12)$$

where ΔV is the volume removed during processing and t is the total processing time.

The maximum feed rate in electrochemical milling using tools A and B were 1.5 mm/min and 1.7 mm/min, respectively. The MMRs in machining a slot using tools A and B were 18.8 mm³ min⁻¹ and 21.2 mm³ min⁻¹, respectively, as shown in Fig. 12. Thus, the results of the electric field simulation were confirmed experimentally.

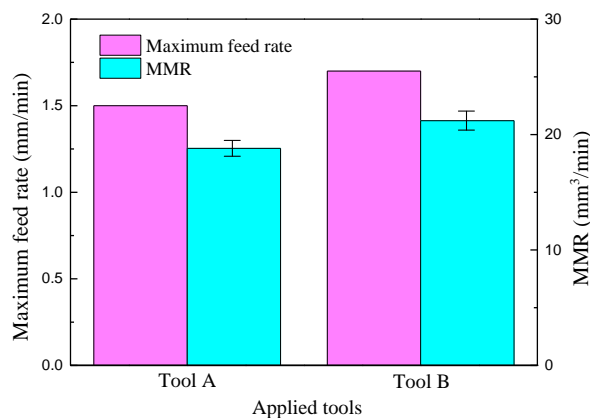


Figure 12. Maximum feed rate and MRR for both tools

Then a slot was electrochemically milled with tool B at a feed rate of 1.7 mm/min. The current density was about 90 A cm^{-2} , which is much bigger than 5 A cm^{-2} . Finally, a small amount of material was removed from the slot sidewall with ECG using tool C. The amount of material removed was 0.19 g, only 6.85% of the total amount removed in both stages.

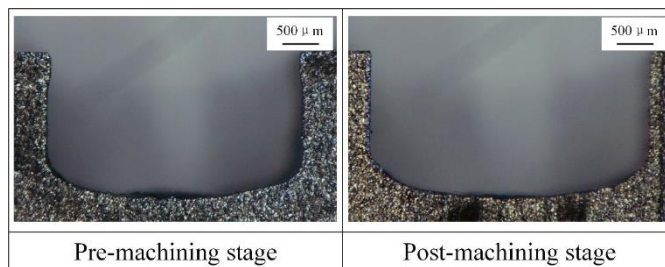


Figure 13. Photographs of cross sections of slots after electrochemical milling and after ECG

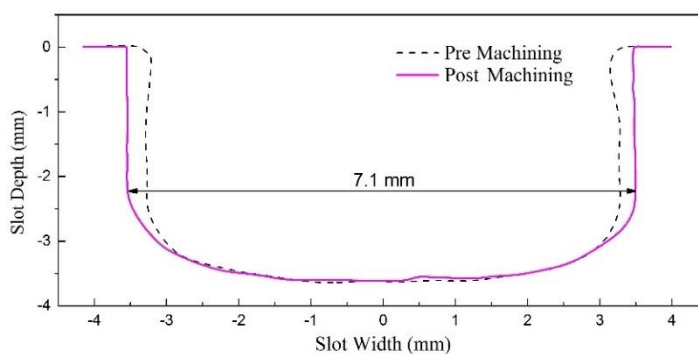


Figure 14. Cross-sectional profiles of slots after electrochemical machining and ECG

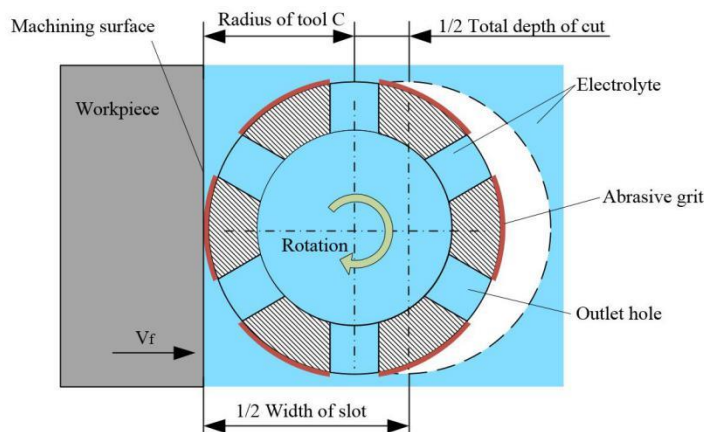


Figure 15. Schematic diagram of ECG showing that there is no machining gap

Fig. 13. shows cross sections of samples 15 mm from the slot entrance. After the electrochemical milling, there are visible bulges and a depression. Obviously, after ECG, the profile of the slot was homogenized effectively.

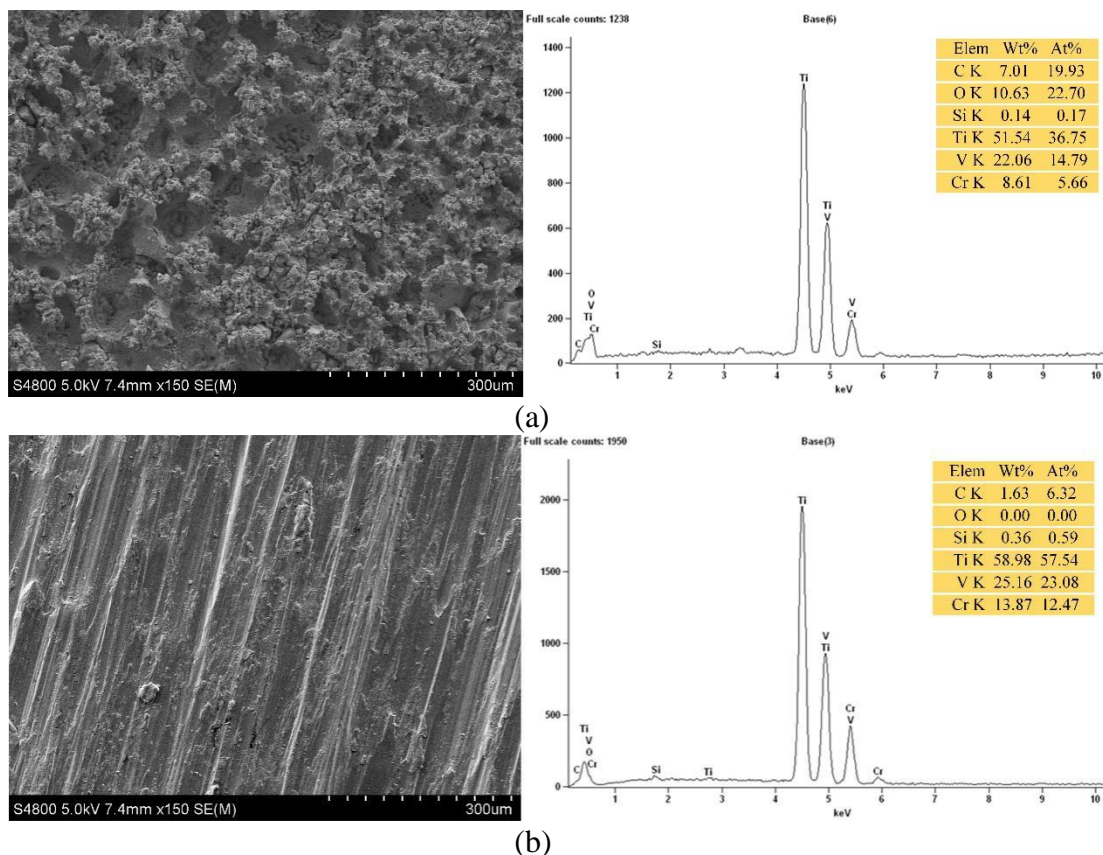


Figure 16. SEM and EDX results for the sidewalls of slots machined by (a) electrochemical machining using tool B and (b) ECG using tool C

Cross-sectional profiles of slots obtained by electrochemical milling and ECG are shown in Fig. 14. It is clear from the profiles that the sidewall flatness was significantly improved after ECG. The average sidewall flatness had decreased from 109.7 μm to 59.0 μm , where the average sidewall flatness is defined as half of the difference between the maximum and minimum slot widths.

Besides, notice that the width of the machined slot (7.1 mm) is equal to the average diameter of tool C (6.2 mm) plus the total depth of cut (0.9 mm) in grinding, which indicates that there was no machining gap. Therefore, this proves that ECG produces only a little overcut, possibly even none, as shown in Fig. 15.

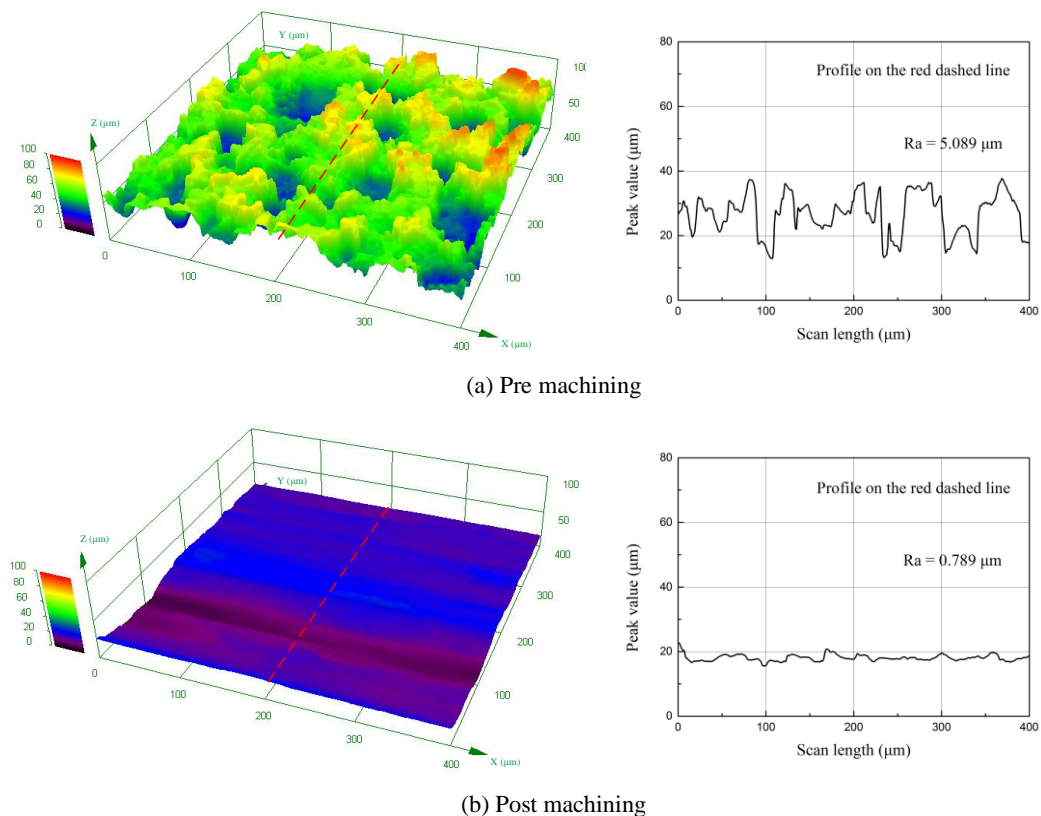


Figure 17. Surface roughness of sidewalls machined by (a) electrochemical milling and (b) ECG

As shown in Fig. 16, SEM was used to determine the surface morphology of the sidewalls machined by electrochemical milling and by ECG. After electrochemical milling, many deep and extremely irregular pits can clearly be observed on the sidewall, which make the surface rough (see Fig. 16a). In comparison, the features on the surface machined by ECG are mainly striations along with other defects, such as smearing and redeposited chips (see Fig. 16b), which are typical surface defects produced by grinding difficult-to-machine materials [27]. Furthermore, almost no pitting corrosion can be observed on the surface machined through ECG, which indicates the absence of electrochemical corrosion in ECG and consequently proves that the removal of material in ECG is mainly due to grinding.

EDX gives similar results. The composition of the surface machined through electrochemical milling is shown in Fig. 16a. Compared with the elemental composition of the matrix shown in Table 2, notice that the O and C contents have significantly increased to 10.63 and 7.01 wt%, respectively. The presence of O and C indicate the formation of an oxidation film. However, as shown in Fig. 16b, only 1.63 wt% of C and almost no O were detected on the surface machined by ECG. This indicates that the oxidation film formed in electrochemical milling can be eliminated effectively by ECG, in which little electrochemical corrosion occurs. It also proves that in ECG the material is removed by grinding rather than electrochemical corrosion. Since physical contact between material and tool is necessary in grinding, this confirms that no overcutting occurs in ECG [28]. It can thus be concluded that, compared with single electrochemical milling, which causes a certain amount of overcut, combined electrochemical milling and ECG allows better control of the machining profile.

The ground surface morphologies of sidewalls machined by electrochemical milling and ECG are shown in Fig. 17. Obviously, the surface roughness was significantly lower after ECG. The ground surface roughness was $Ra = 0.789 \mu\text{m}$, which is an 84.5% improvement compared with electrochemical milling.

4. CONCLUSIONS

This article presents a method of machining Ti40 titanium alloy using electrochemical milling followed by ECG and studies the performance of the combined method. The basic electrochemical properties of Ti40 titanium alloy in NaNO_3 solution were investigated. Slots were machined with high efficiency and good surface quality. The conclusions can be drawn as follows:

(1) In electrochemical milling, sparks occur with tools with a sharp edge. In comparison, a rounded corner increases the inter-electrode gap and, thus, the maximum feed rate.

(2) From the polarization curve, the measured dissolution potential of Ti40 titanium alloy in 10% NaNO_3 solution at 30°C was 4.5 V. The current efficiency curve showed that dissolution occurs efficiently at a relatively high current density (more than 5 A cm^{-2}).

(3) In electrochemical milling with tool B, the maximum feed rate was 1.7 mm min^{-1} when the applied voltage was 15 V. Slots were machined at the maximum feed rate and the MMR was $21.2 \text{ mm}^3 \text{ min}^{-1}$. The depth of cut was 3 mm.

(4) The uneven profile and rough surface of the sidewall machined via electrochemical milling was observably improved by ECG. Compared with electrochemical milling, the average sidewall flatness decreased from $109.7 \mu\text{m}$ to $59.0 \mu\text{m}$ and the sidewall surface roughness decreased from $5.089 \mu\text{m}$ to $0.789 \mu\text{m}$. The mass of the material removed by ECG was small, accounting for only 6.85% of the total material removed. Besides, no overcuts could be detected in the final surfaces.

(5) The oxidation film formed in electrochemical milling can be effectively eliminated by ECG. The carbon content decreased from 7.01 wt% to 1.63 wt%, and the oxygen content decreased from 10.63 wt% to 0 wt%.

ACKNOWLEDGEMENTS

This work was supported by the National Natural Science Foundation of China (grant 51875286) and the Postgraduate Research & Practice Innovation Program of Jiangsu Province (grant KYCX18_0263).

References

1. D.S. Liu, J.H. Xu, W.F. Ding, Y.C. Fu, C.Y. Yang and H.H. Su, *J. Mater. Process. Technol.*, 229 (2016) 641.
2. Y.L. Lai, P.X. Zhang, S.F. Zhang, K.X. Wang, Q. Lei, S.W. Xin, Y.J. Zheng and Q.M. Tan, *J. Aeronaut. Mater.*, 37 (2017) 22.
3. Y.Q. Zhao, L. Zhou and J. Deng, *Rare Met. Mater. Eng.*, 28 (1999) 77.
4. F. Klocke, A. Klink, D. Veselovac, D.K. Aspinwall, S.L. Soo, M. Schmidt, J. Schilp, G. Levy and J.P. Kruth, *CIRP Ann. Manuf. Technol.*, 63 (2014) 703.

5. Z.W. Zhu, D.Y. Wang, J. Bao, N.F. Wang and D. Zhu, *Int. J. Adv. Manuf. Technol.*, 80 (2015) 1957.
6. M.H. Wang, W. Peng, C.Y. Yao and Q.F. Zhang, *Int. J. Adv. Manuf. Technol.*, 49 (2010) 969.
7. Z.Z. Gu, W.G. Zhu, X.H. Zheng and X.M. Bai, *Int. J. Adv. Manuf. Technol.*, 100 (2018) 857.
8. C.S. Chang and L.W. Hourng, *J. Appl. Electrochem.*, 31 (2001) 145.
9. F. Klocke, M. Zeis, S. Harst, A. Klink, D. Veselovac and M. Baumgärtner, *Procedia CIRP*, 8 (2013) 265.
10. G.X. Liu, H.P. Luo, Y.J. Zhang, J. Qian and J.W. Liu, *Int. J. Adv. Manuf. Technol.*, 85 (2016) 191.
11. S. Niu, N.S. Qu, S.X. Fu, X.L. Fang and H.S. Li, *Int. J. Adv. Manuf. Technol.*, 93 (2017) 2123.
12. D.Y. Wang, B. He and W.J. Cao, *Appl. Sci.*, 9 (2019) 690.
13. X.L. Fang, N.S. Qu, Y.D. Zhang, Z.Y. Xiu and D. Zhu, *J. Mater. Process. Technol.*, 214 (2014) 556.
14. R.N. Goswami, S. Mitra and S.K. Sarkar, *Int. J. Adv. Manuf. Technol.*, 40 (2009) 729.
15. S. Zaborski, M. Lupak and D. Poros, *J. Mater. Process. Technol.*, 149 (2004) 414.
16. A. Hasçalık and U. Çaydaş, *J. Mater. Process. Technol.*, 190 (2007) 173.
17. S. Li, Y. Wu, K. Yamamura, M. Nomura and T. Fujii, *CIRP Ann. Manuf. Technol.*, (2017) S0007850617300896.
18. D. Zhu, Y.B. Zeng, Z.Y. Xu and X.Y. Zhang, *CIRP Ann. Manuf. Technol.*, 60 (2011) 247.
19. X.F. Zhang, N.S. Qu, H.S. Li and Z.Y. Xu, *Int. J. Adv. Manuf. Technol.*, 81 (2015) 1475.
20. X.C. Jiang, J. Liu, D. Zhu, M.M. Wang and N.S. Qu, *Appl. Sci.*, 8 (2018) 1296.
21. N.S. Qu, Y. Hu, D. Zhu, and Z.Y. Xu, *Mater. Manuf. Process.*, 29 (2014) 572.
22. L. Tang and Y. F. Guo, *Mater. Manuf. Process.*, 28 (2013) 457.
23. S.S. Anasane and B. Bhattacharyya, *Int. J. Adv. Manuf. Technol.*, 86 (2016) 1.
24. D. Sazou, K. Saltidou and M. Pagitsas, *Electrochim. Acta*, 76 (2012) 48.
25. Y. Liu and N.S. Qu, *Journal of The Electrochemical Society*, 166 (2019) E35.
26. J. Li, H.S. Li, X.Y. Hu, S. Niu and G.L. Xu, *Appl. Sci.*, 10 (2020) 1941.
27. N. Qian, W. Ding and Y. Zhu, *Int. J. Adv. Manuf. Technol.*, 97 (2018) 1649.
28. G.Q. Liu, H.S. Li, S. Niu, X.K. Yue and N.S. Qu, *Int. J. Electrochem. Sci.*, 14 (2019) 9876.

© 2020 The Authors. Published by ESG (www.electrochemsci.org). This article is an open access article distributed under the terms and conditions of the Creative Commons Attribution license (<http://creativecommons.org/licenses/by/4.0/>).